

A Deep Learning Approach to Private Data Sharing of Medical Images Using Conditional GANs

Hanxi Sun*

Purdue University, Department of Statistics
West Lafayette, IN, USA

Jason Plawinski*

Novartis
Basel, Switzerland

Sajanth Subramaniam

Novartis
Basel, Switzerland

Amir Jamaludin

Oxford Big Data Institute
Oxford, UK

Timor Kadir

Oxford Big Data Institute
Oxford, UK

Aimee Readie

Novartis
East Hanover, NJ, USA

Gregory Ligozio

Novartis
East Hanover, NJ, USA

David Ohlssen

Novartis
East Hanover, NJ, USA

Mark Baillie†

Novartis
Basel, Switzerland

Thibaud Coroller†‡

Novartis
East Hanover, NJ, USA

Abstract

Sharing data from clinical studies can facilitate innovative data-driven research and ultimately lead to better public health. However, sharing biomedical data can put sensitive personal information at risk. This is usually solved by anonymization, which is a slow and expensive process. An alternative to anonymization is sharing a synthetic dataset that bears a behaviour similar to the real data but preserves privacy. As part of the collaboration between Novartis and the Oxford Big Data Institute, we generate a synthetic dataset based on COSENTYX® (secukinumab) Ankylosing Spondylitis (AS) clinical study. We apply an Auxiliary Classifier GAN (ac-GAN) to generate synthetic magnetic resonance images (MRIs) of vertebral units (VUs). The images are conditioned on the VU location (cervical, thoracic and lumbar). In this paper, we present a method for generating a synthetic dataset and conduct an in-depth analysis on its properties of along three key metrics: image fidelity, sample diversity and dataset privacy.

1. Introduction

In recent years, deep learning has become an indispensable tool for clinical images analysis, from ophthalmology[1], pathology[2] to medical images[3, 4]. By the end of 2020, PubMed[5] has a total of 9,497 entries for “deep learning + image” with more than half of them published in 2020. While the number of publications using such techniques has exploded, the number of publicly available datasets has not. This research area has an unsatisfied thirst for larger and larger datasets to tackle future arduous tasks. A lack of data availability also impacts reproducibility. For example, most method papers are not published with the corresponding research data, which would allow other scientists to validate and verify results. Moreover, to solve problems in the biomedical space, often large, pooled datasets are required that may span multiple institutions. Sharing data enables scientific progress, but sharing data is challenging due to privacy[6], ethical[7], legal[8], and institutional challenges[9]. However, a solution would facilitate collaboration across research groups allowing the possibility to reproduce and build upon existing work. This can be supported by having access to code and data.

While replication[10] of hypotheses is the key to scientific understanding in the biomedical field, it is typically hindered by the need to access and analyse multiple data sources. Despite efforts to share data[11], there is a lack of labelled datasets on which to build novel models. Using

*Co-first authors

†Co-last authors

‡Corresponding author: thibaud.coroller@novartis.com

a risk based approach to anonymizing data[12], which is a process to remove or reduce information that will in turn reduce the risk of an individual being identified, is an option but it is a complex and laborious task. One part of the process is to ensure that all information that could directly identify an individual is removed. While this is difficult enough for tabular data, it becomes even more challenging for images due to the complexity of the meta information and the need to exhaustively check each slide of the image for pixel-burnt information (e.g. patient name).

Other parts of the anonymization process can reduce data utility, which has a knock-on effect on the quality of subsequent research. Open scientific collaboration comes at a tension with the federation and control of sensitive data. Data sharing contributes to scientific understanding in an open and collaborative spirit. However, sharing data could have consequences if it was not properly approved (non-anonymized datasets, lack of patient agreement) or if it is leveraged for unintended uses. This illustrates the need for other data (including models) sharing methods that would protect scientists from this dilemma.

One solution is called federated learning[13] where instead of sharing data, a model is being shared across scientists to be trained their private datasets rather than pooling datasets in a single location. It allows researchers to efficiently train a model across restricted datasets but is rather complex to setup to ensure efficient model training and tackling of security concerns. Another solution could be to share a synthetic version of a sensitive dataset that preserves global properties (for example their association to a specific clinical variable) while preserving patients privacy. While nothing will ever replace an actual dataset, this approximative version of it could already help solve important research steps. For example, one could use such a dataset to prototype new methods (define model architecture). Furthermore, if this approximation could be generated in a quick and effortless way, it could become a viable option for increasing data need for nowadays models. This provides opportunities for changing how data is shared, provides sufficient control for data custodians, while allowing for the pooling and integration of disparate data sources to be used to answer complex questions.

In this paper we propose a method that uses generative adversarial networks (GANs)[14] to create synthetic images while conserving its association with clinical variables as shown in Figure 1. A synthetic dataset should have three core properties, namely fidelity, diversity and privacy, before it can be externally shared as a substitute for the original dataset. It should reproduce realistic samples in comparison to the original dataset (fidelity), the samples should exhibit similar variations as the original dataset (diversity), and the original samples should not be retrievable from the synthetic dataset (privacy).

2. Results

To demonstrate the effectiveness of the proposed method pGAN we use it for creating a synthetic dataset of T1 magnetic resonance images (MRIs) of vertebral units (VUs) labelled with VU location regions such as cervical, thoracic and lumbar. The quality of the synthetic dataset is evaluated from the aforementioned three key metrics.

2.1. Fidelity

The first assessment is to evaluate whether the synthetic VUs are visually indistinguishable from real VUs for a given location. Figure 2-A shows a collection of real and synthetic data. Visually, synthetic samples look like real ones and expose different structures depending on their conditioned region location (i.e. cervical, thoracic and lumbar). Inspired from recent work on face morphing with GANs[15], we show in Figure 2-B that we can control generator behaviour by continuously changing the condition vector c . We do so using a linear interpolation between the source and target region wanted. This demonstrates that our generator is correctly conditioned and can create specific VU locations on demand.

2.2. Diversity

We evaluate whether the real and synthetic dataset have similar global distribution while having distinct individual VU samples as shown in Figure 3-A. To obtain a meaningful low dimensional representation we apply a UMAP[16] transform to our dataset of VUs. UMAP is a powerful non-linear dimensionality reduction technique. It is similar under many aspects to t-SNE[17] but differs by the fact that the transformation from high dimension to low dimension is learnable. We leverage this by training the UMAP only on real data and then applying the transform to unseen real data as well as synthetic data.

Our first finding is that VU location distribution is separable and similar between real and synthetic samples, showing that both datasets have similar global distribution. The second finding is that the synthetic VUs cover most of the distribution in the low dimensional representation space without overlapping with real VUs implying that the synthetic samples are indeed distinct. Those findings confirm that our GAN can synthesize data that behaves like real VU and that its diversity (phenotypic differences) matches the real distribution as we do not observe mode collapse.

We further examine the quality of the synthetic dataset in terms of its capability to serve as a functional equivalent to a real dataset for downstream training tasks by training two ResNet-18[18] based classifiers F_{real} and F_{synth} with real and synthetic data respectively. Figure 3-C shows the ROC curves for both classifiers. We observe that, while F_{synth} slightly underperforms compared to F_{real} , the syn-

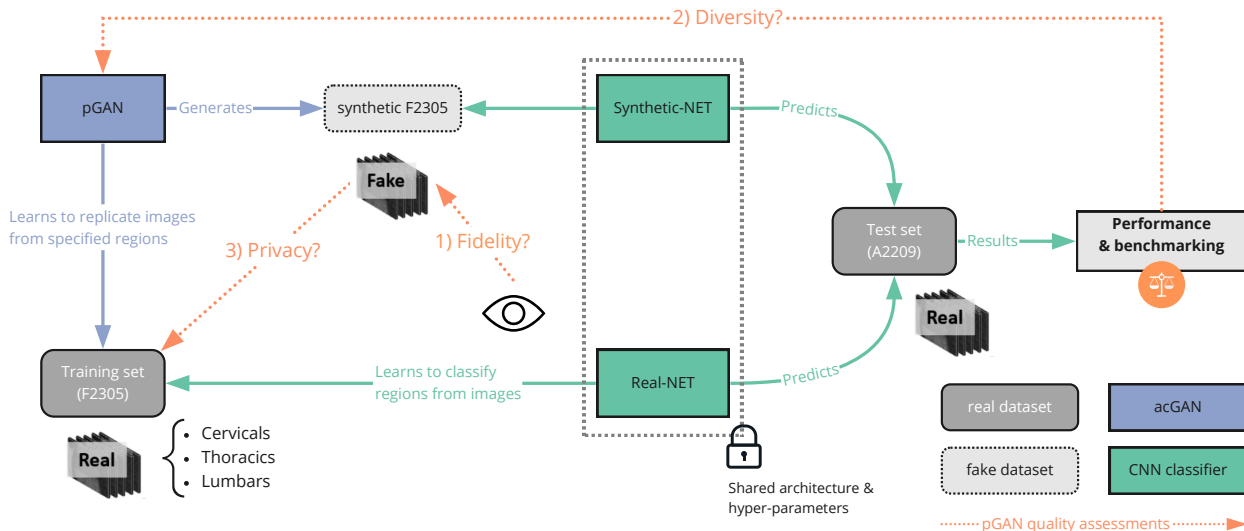


Figure 1: Overview of the privacy computing workflow to share synthetic medical images (vertebra MRIs) our privacy GAN model (pGAN). We trained an auxiliary classifier generative adversarial network (acGAN) from a dataset composed of vertebra images alongside their corresponding locations (cervical, thoracic, lumbar). Then, we use our trained pGAN model to generate a synthetic dataset of vertebra. The quality of the output synthetic dataset was evaluated based on three criteria (privacy, fidelity and diversity). Once all criteria passed, we could safely share those synthetic data with external scientists without any privacy risk while retaining all data usefulness.

thetic dataset can approximate the distribution in the original data when tested for VU region. The slight discrepancy in performance is to be expected as the conservation of privacy can be expected to come at a cost in data quality. While, in principle, the performance of F_{synth} could asymptotically reach the one of F_{real} , in practice there is a trade-off between overfitting the training set and replicating the classification statistics of a network trained solely on the training set.

2.3. Privacy

We define a privacy leakage as finding traces of the training dataset within the synthetic dataset. In this section, we restrict the study to only sharing a synthetic and finite dataset rather than the trained generative model itself. This restriction makes privacy attacks much more difficult because they cannot be conducted by reverse engineering the network’s output and there is no direct access to the generative model’s latent space. This means only attacks that rely on directly comparing candidate images with the synthetic dataset can jeopardize privacy. An obvious case of privacy threatening behaviour in GAN is overfitting. A major overfitting corresponds to a generator outputting synthetic images that are exact copies from training images. Other convergence issues can be problematic as well such as cases where

the generator only learns to reproduce a few number of samples from the training set (mode collapse).

We identified two main potential vulnerabilities for a synthetic dataset:

- **Pairwise attacks:** where finding a synthetic image which is similar to a given sample would prove that this sample was used during training.
- **Distribution attacks:** where a high density of synthetic images cluster around one or a few real images.

To assess the robustness to these attacks, we simulate them by using a “candidate dataset” (supplementary Figure S1) and evaluate which ones can be traced back to the training set.

2.3.1 Robustness to pairwise attacks

For robustness to pairwise attacks, we compute the similarity between a candidate sample and all the images from the synthetic dataset. A relatively small L2 distance may indicate that the candidate was used for the generator training. The distribution of minimum distances between candidate and synthetic images are represented in Figure 4-A. On this graph, we would expect the lowest distances to be train-synthetic pairs and the largest ones to be test-synthetic

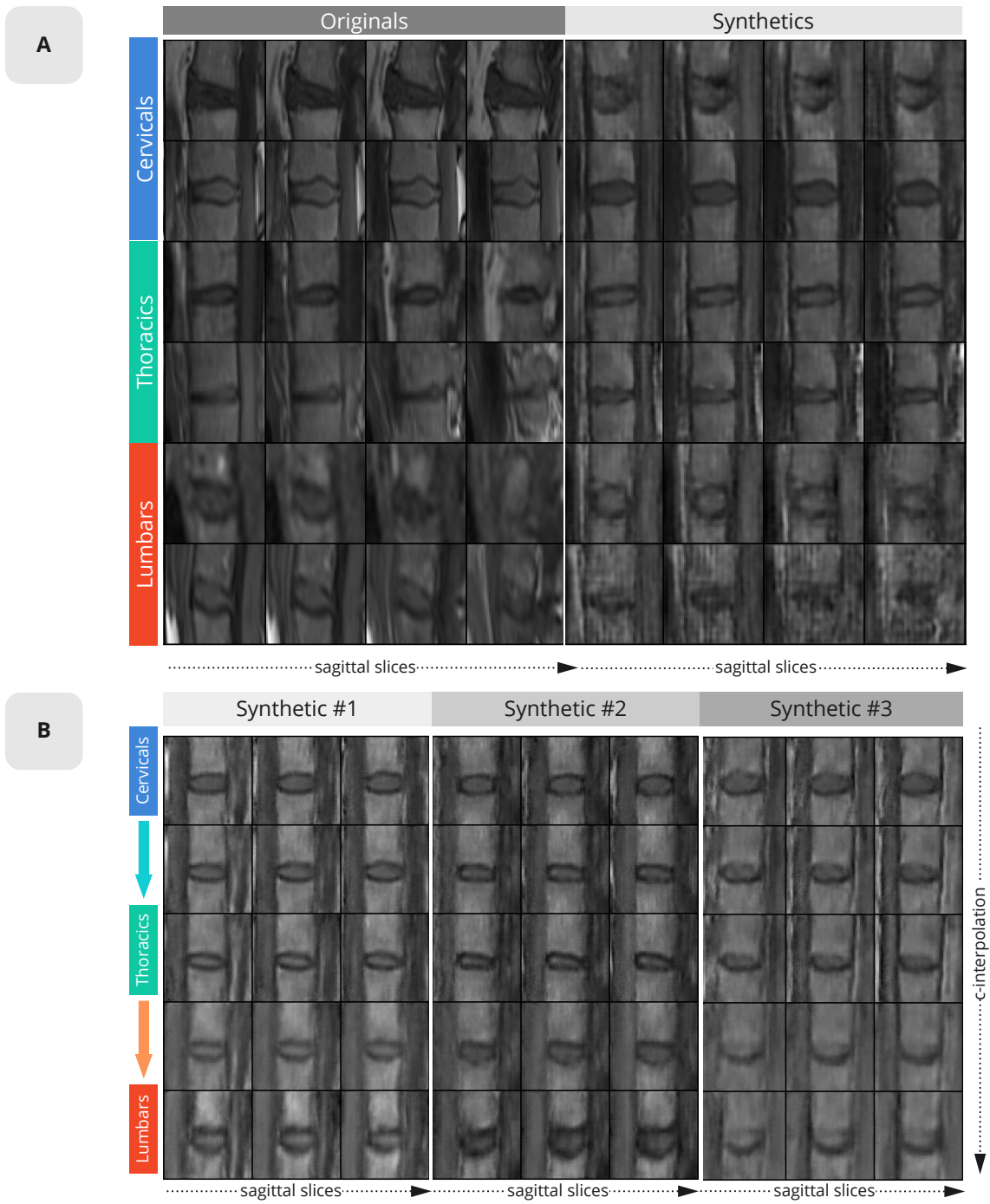


Figure 2: A) Examples of real and synthetic vertebrae and their corresponding vertebrae units (VU) locations. Each row shows 4 consecutive vertical slices for a real and fake VU (each slice is of size 64x64). The first two rows are cervical VUs, followed respectively by thoracic and lumbar. B) Morphing an image from one location to another was done by interpolating the condition c while keeping the latent variable z untouched. Here we are using a single step $n = 1$ for each morphing such that the shown intermediate states correspond to a 50%/50% morph between two locations.

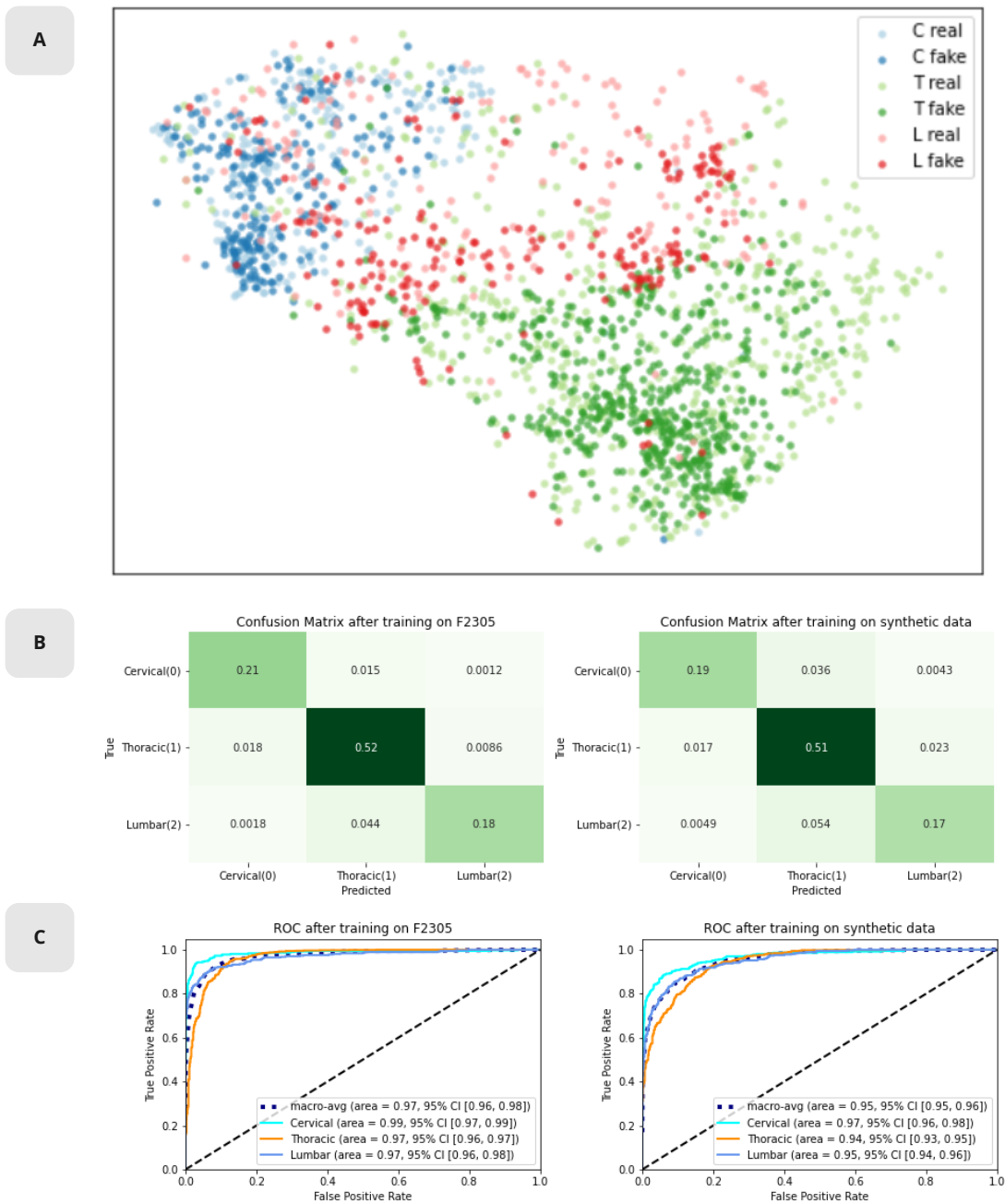


Figure 3: A) Low dimensional UMAP representation of real and synthetic vertebra units locations cervical, thoracic and lumbar labelled as blue, green and red respectively. B) Confusion matrices of F_{real} (left) and F_{synth} (right) when tested on A2209. The predicted class for a sample image x_i corresponds to $\max(F_{\text{real}}(x_i))$ and $\max(F_{\text{synth}}(x_i))$ respectively. The class distribution of the test set corresponds to $(p_C, p_T, p_L) = (0.23, 0.55, 0.23)$. C) ROC and AUC for F_{real} (left) and F_{synth} (right) when tested on A2209. Every class specific ROC curve was computed by treating the other two classes as negative instances, effectively reformulating the classification for each class as a binary problem.

due to some overfitting behaviour from the GANs. In the privacy-threatening scenario, images from training are easy to identify by a simple anomaly detection task. An anomaly detection with reference distances is available on supplementary Figure S2. On our observed synthetic dataset however, it is impossible to reliably identify candidates originating from training from the ones coming from validation. This is also confirmed using an embedding space obtained applying a UMAP. Our synthetic dataset hence shows robustness to pairwise attacks, in both pixel and embedding space.

2.3.2 Robustness to distribution attacks

To evaluate the robustness to distribution attacks, we identify clusters of synthetic images around a given candidate. The clusters are defined by counting the number of synthetic images in the candidate neighbourhood and the results are shown in Figure 4-B. We expect large cluster to form around candidates from the training set and other candidates to have a small number of neighbours. The privacy-threatening scenario (left figures) reflects this hypothesis. The observed behaviour of the synthetic data is shown on the two most right figures. Candidates from the test set rarely belong to large clusters unlike candidates from training or validation. In fact, the largest clusters overwhelmingly form around training samples. Even if this method can help identify a handful of training example it is ineffective for most of them. Indeed, the size of the training set and the synthetic dataset are around the same (around 10'000 samples). This means that on average, one training sample can be only traced back to one synthetic sample. This means that by construction, our synthetic dataset is safe from distribution attacks.

It is also worth noting that the embedding space is not uniformly populated. As seen on Figure 4-C, high density of synthetic images is in general linked to a high density of real images (blue dots on the figure) and not due to the GAN generation collapsing and only generating one type of sample. A detailed detection of training samples is available in the supplementary material Figure S3, Figure S4 and Table S1.

3. Discussion

Sharing data across research groups and institutions provides an opportunity to answer complex questions through the pooling of information and resources. However, there is a need to share data safely and faster. Sharing synthetic dataset overcomes the privacy and legal barriers to enable efficient collaborations. We propose generating synthetic datasets of labelled medical images with a type of GAN model. Our result satisfies:

- **Fidelity:** We produce realistic medical images and

labels. Generated images are satisfying user defined conditions (spinal region)

- **Diversity:** The synthetic dataset preserves the analytical behaviour of the real data. Generated data has a similar distribution than real data in term of variations.
- **Privacy:** When only the synthetic dataset is shared, real data are protected from identification. No real data can be identified from synthetic only nor limited access to real data (data leakage).

Data privacy protection in the age of data science and artificial intelligence has drawn a lot of attention, especially in the medical field[19]. One major way of attacking privacy is membership inference attack[20], which aims to determine whether data from a target patient is included in the study. A general approach to protect data from such attacks is differential privacy[21], which masks real data with a carefully designed noise during training. It provides a strong protection of privacy and has been applied in a variety of problems, including synthetic data generation with GAN[22, 23, 24]. With differential privacy, privacy is protected with the cost of sample quality and diversity of the synthetic dataset. However, adding noise is not a satisfying solution to our problem as it biases the synthetic distribution and, on images, noise only alters mathematical similarities while keeping general shapes and image content intact. This makes noise-based methods a particularly poor fit for image privacy.

Besides privacy protection, GAN has also been used in medical research, often as a data augmentation approach[25, 26], see for instance [23, 27, 28, 29, 30, 31]. For this work we used a dataset of MRI spine images with VU location labels (cervicals, thoracics and lumbar). We succeeded in creating a synthetic dataset by using an AC-GAN to generate synthetic samples with their respective location labels. The synthetic dataset can safely be shared as a surrogate for the real dataset because it meets the consistency and privacy criteria. The synthetic samples are realistic and bear high visual quality of samples. The behaviour of the real dataset was replicated and dataset wide analysis such as classification (trained from scratch) performed to a similar level on both the synthetic and the real dataset. No sample from the synthetic dataset can be associated to a sample from the real dataset making it impossible to trace back patient information from a synthetic sample.

This work provides a general tool for privacy protection when collaborating on medical datasets. For instance, the synthetic MRI spine images could be used for developing and testing new prediction and classification models across institutions, for training readers / reviewers of MRI, etc. We do not benchmark our results against pure differential privacy (like additive Laplacian noise) because the effec-

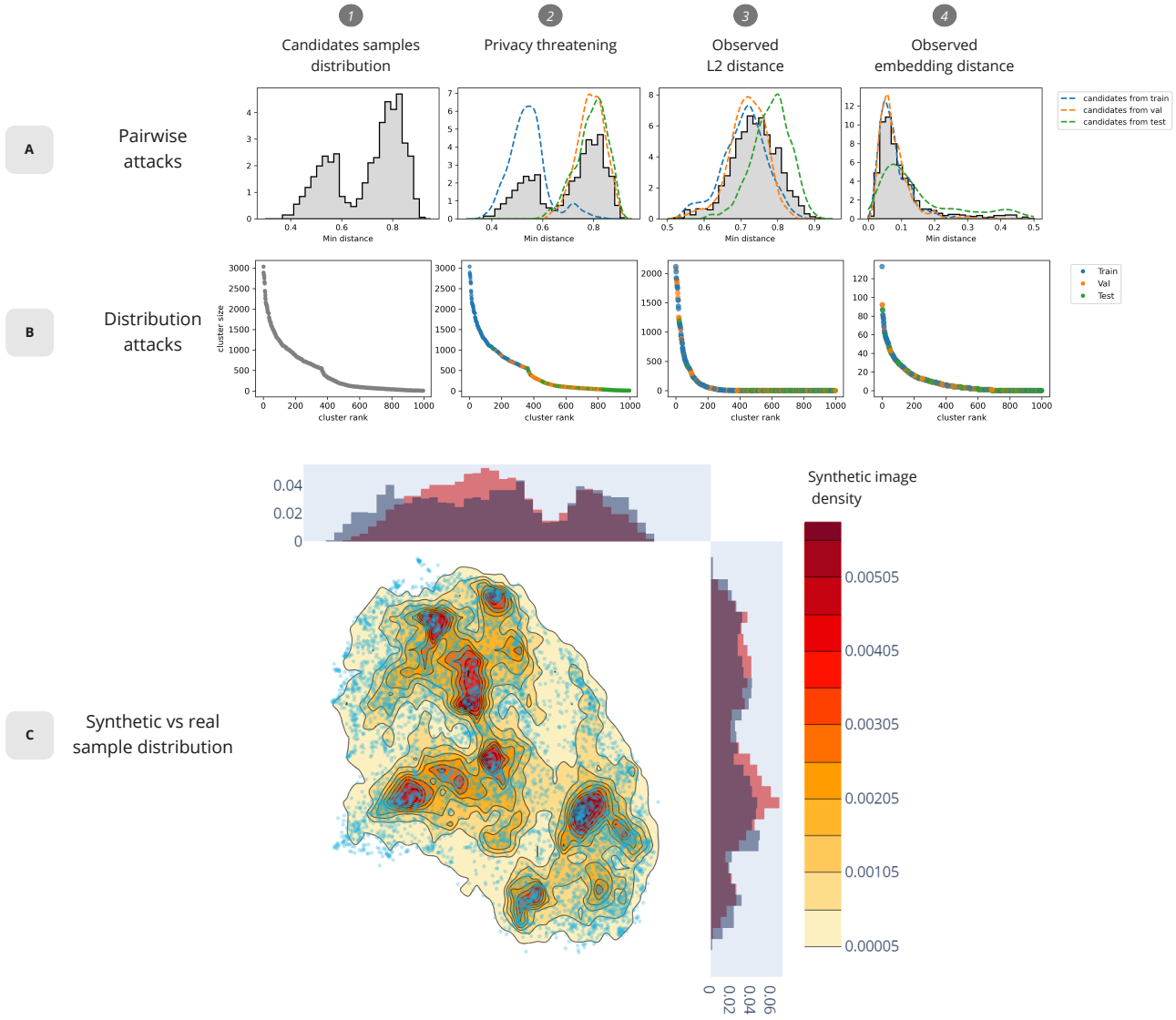


Figure 4: A) **Simulation of pairwise attacks.** A small distance indicates that the candidate is likely from the training set. 1-2 are toy examples of privacy threatening scenario with easily identifiable candidates from training. 3-4 are the observed behavior of our synthetic dataset. B) **Simulation of distribution attacks.** Large cluster indicates that the candidate is likely coming from the training set. 1-2 are privacy threatening and 3-4 are observed behavior on the synthetic dataset. C) 2D projection of the synthetic and training dataset. Shades of yellow-red are density levels of synthetic images and blue dots are individual training examples.

tiveness of such methods can be mitigated by CNN denoisers which would require an investigation on its own. We only evaluate privacy through the re-identification of training samples (by outlier detection) which, in our case, is the only potential type of attack. Our results show that GANs do not replicate samples from the training set and tend to be robust to pairwise attacks. The presence of artifacts, for example, affects the similarity measures in pixel space ren-

dering the comparison of real and synthetic samples particularly difficult. Comparing in feature space does not solve the problem because the only embedding space where synthetic and training images share similar features is the GAN embedding space itself. Density attacks seem to be more dangerous than pairwise attacks because it does not require an exact match between a synthetic and a candidate sample. Simply having multiple synthetic images that are like

a candidate image could already be enough to conclude on its origin. Thankfully, our synthetic dataset is robust to density attacks. With around 1.2 synthetic data point per real data point, our synthetic dataset is too small to create meaningful clusters. This means clusters will either be large but not discriminative and composed by images barely similar images or too small to be relevant.

4. Limitations

Ensuring privacy is a challenging aspect of this project, as defining a robust method to assess similarity between images is complex[32]. Due to sample size limitation, we only investigated generating VUs instead of full spines images, for computing efficiency, we resampled the images to a smaller format. We also tried conditioning the AC-GAN on clinical metrics but the imbalance between the number positive samples and negative samples as well as the intra-reader discrepancies led to similarly noisy results that proved too hard to analyse. Finally, in our approach the synthetic dataset has a fixed privacy tolerance that is a factor of the real dataset and the GAN convergence but cannot be modulated based on specific needs.

5. Future steps

Even though the synthetic dataset produced in this evaluation does not contain synthetic samples close to real samples, the generator can theoretically create such images. It is unlikely to happen as the curse of dimensionality greatly reduces the probability of sampling an image with the exact same parameters as the real data. However, having to check that the network did not reproduce a real sample after each generation is inefficient. A direction for further research could be to learn where the real images lie in the latent space of the generator and then create a careful sampling strategy to avoid sampling around these points. Another research direction that is considered is to condition the generation process not only on a few classes but on large tabular data (such as clinical and demographic data). In fact, the current architecture would have to change significantly. Another step of privacy preserving synthetic generation, this time of tabular data would be necessary. Additionally, the loss function of the AC-GAN does not behave well with soft labels and conditions with small or no correlation with the content of the images. On the spine dataset, a useful feature would also be to generate a full spine and instead of independent VUs. Finding a good trade-off between VUs consistency and memory is important however since generating 21 VUs at once is extremely memory intensive and only a weak correlation would be required.

6. Methods

6.1. Dataset descriptions

Two datasets were used in the study:

- **F2305 (MEASURE1):** The study evaluated the effect of secukinumab, a fully human anti-interleukin-17A monoclonal antibody, on efficacy, imaging outcomes, and safety through 4 years (208 weeks) in patients with Ankylosing Spondylitis (AS). Through 4 years, secukinumab provided sustained efficacy on signs and symptoms, and MRI outcomes, a low rate of radiographic progression and a consistent safety profile. This was the first study reporting longer-term effect of secukinumab on radiographic structural progression in AS[33].
- **F2209:** The phase II pre-filled syringe testing study evaluated the use of secukinumab for the treatment of AS.

Analysis dataset included 108 patients from the secukinumab MEASURE 1 (F2305) study, in which imaging was done using T1 and STIR sagittal MRI at baseline and weeks 16, 52, 104, 156 and 208. STIR images were not included in this study. Regardless of their acquisition date all T1 were pooled, then we extracted 23 vertebra units (VU: section between two adjacent vertebrae) using SpineNet[34]. F2305 was used for the training and validation, with respectively 7832 and 2205 vertebral units (VUs). The validation set and training set are split so that there is no overlap of patients in both sets. A2209 has 1625 VUs and was used solely for testing purposes. Each VUs was pre-processed to have 9 slices (4 before and after from the central one) and labelled according to their anatomical regions (cervical, thoracic and lumbar). VUs from the sacrum were excluded from the pooled dataset. All VUs were rotated to align the VUs together (vertical line) and zoomed to have consistent size-ratio across VUs.

6.2. Auxiliary classifier Generative adversarial networks (AC-GAN)

We use auxiliary classifier generative adversarial networks (AC-GAN)[35] to generate synthetic VUs and associated VU regions. AC-GAN is a variation of generative adversarial networks (GAN) that relies on the competition between two deep neural networks, the generator and discriminator, to create realistic images. Figure 5 shows the general structure of the AC-GAN model.

The training is done by iteratively improving the generator and discriminator. The loss consists of two components, the discriminative loss L_D on distinguishing between real and fake images and an α weighted classification loss L_C

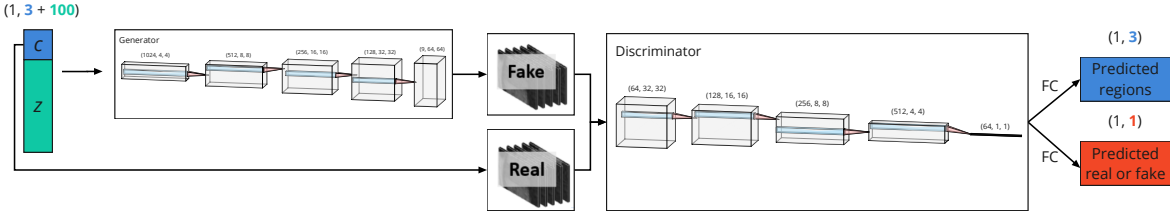


Figure 5: **The AC-GAN structure.** The generator (G) is a deep neural network that transforms a feature vector of the class label (c) and a random noise (z) to an image, and the discriminator (D) distinguishes between the real images and fake images and also predicts the class labels for each image.

in the accuracy of predicting class labels, i.e.

$$L = L_D + \alpha L_C$$

where

$$L_D = E [\log P(\text{real}|X_{\text{real}})] + E [\log P(\text{fake}|X_{\text{fake}})]$$

$$L_C = E [\log P(\hat{c} = c|X)]$$

- **Pre-processing:** we keep the same 9 slices of VUs and rescale each slice from 112x224 to 64x64. For this specific dataset of VUs, although being 3D images, VUs are treated as 2-dimensional images with 9 channels and learnt with a 2D AC-GAN model, as the 3-dimensional structure in VUs are not very strong due to large slice thicknesses.
- **Feature vector:** apart from the additional 3 dimension for class labels (region encoded as a length 3 one-hot vector), we used a 100-dimensional standard Gaussian random noise as the input to the generator.
- **Generator:** the generator consists of five 2-dimensional deconvolutions (transposed convolution) layers with 512, 256, 128, 64 and 9 output channels, respectively. We used a kernel of size 4 in all layers. The first layer has a stride of 1 and 0 padding to up sample the image size from 1x1 to 4x4, then the rest layers are set with stride size 2 and padding 1 to double the image size. Rectified Linear Unit (ReLU) activations were used in the first 4 layers and the hyperbolic tangent (tanh) activation was used in the last layer to restrict the output pixels within the range of [-1, 1].
- **Discriminator:** the discriminator consists of five 2-dimensional convolution layers with 64, 128, 256, 512, 64 output channels, respectively, and each layer is set with kernel size 4. A stride size 2 and padding 1 is used in all layers but the last one, and the last layer is set with stride size 1 and padding 0. Leaky ReLU activations were used in all layers with a negative slope of

0.2. After passing through the convolution layers that extract information from images, VUs are then going through two separate fully connected layers with sigmoid and softmax activation, respectively, to produce the decision of real vs fake as well as the predicted classification label.

- **Loss:** the classification loss is weighted by $\alpha = 1$ during training.
- **Optimization:** Training is done with Adam optimizer[36] with learning rate 10^{-4} for both the generator and the discriminator.
- **Model Selection:** When performing hyperparameter search for training the model, we rely on visual inspection, adversarial and classification loss during training as well as classification on the A2209 test set.
- **Synthetic Data:** to generate the synthetic dataset, we first simulate VU location from the empirical distribution of it in the real data. We then use the sampled VU location to condition the generator and generate the entire image.
 - **Reproducibility:** Trial data used for the GAN training is restricted, but synthetic VU data used for the diversity results are available. Additionally, all Python codes are fully available.

6.3. Real vs. synthetic ResNet-18 performance

Prior to the training of F_{synth} , we created a synthetic dataset using our trained generator. We designed the synthetic dataset size and class distribution to approximate F2305 by generating 10,000 synthetic images whereas the class assignment is sampled from a distribution $(p_C, p_T, p_L) = (0.25, 0.55, 0.2)$ where we denote the probability for cervical, thoracic and lumbar respectively.

We train two ResNet-18 based classifiers F for the VU region. For the first classifier F_{real} we use F2305 as the training set while the second classifier F_{synth} is trained solely on

synthetic data. In both cases, A2209 was used as independent test set. Both models use the same hyperparameters and an identical training procedure.

- Optimization: We use stochastic gradient descent with a learning rate of 10^{-4} and momentum of 0.9. Networks were trained for 20 epochs with a batch of 32.
- Loss: We use the cross-entropy loss.

We compute a single global ROC curve for each classifier by averaging the class specific ROC curves using equal weights (macro-average). The 95 percentile confidence intervals for the AUCs were computed using bias-corrected and accelerated bootstrapping[37] with 2000 resamples.

6.4. Image morphing

To generate our synthetic image, we input a tensor that concatenates a random noise $z \in \mathbb{R}^{100}$ and a condition $c_k \in \mathbb{R}^K$. The tensor c_k is a hot-encoding vector representing the vertebra location

$$c_{k,i} = \delta_{ki}$$

where δ is the Kronecker delta. In the case of $K = 3$ we have

$$\begin{aligned} c_1 &= [1, 0, 0]^T && \text{(cervical)} \\ c_2 &= [0, 1, 0]^T && \text{(thoracic)} \\ c_3 &= [0, 0, 1]^T && \text{(lumbar)} \end{aligned}$$

To morph an image from a location to a new one, we only need to modify our tensor c to impact the generator, thus leaving untouched z . We use linear interpolation between source condition c_k and the target one $c_{k'}$. For n steps we have for step $t \in \{0, 1, \dots, n\}$

$$c_{k \rightarrow k', i}^t = \begin{cases} \frac{n-t}{n}, & \text{if } i = k \\ \frac{t}{n}, & \text{if } i = k' \\ 0, & \text{otherwise} \end{cases}$$

Using this definition, we have for morphing from cervical to lumbar at step t

$$c_{1 \rightarrow 3}^t = \frac{1}{n} \begin{bmatrix} n-t \\ 0 \\ t \end{bmatrix}$$

6.5. Privacy

To evaluate privacy, we created a list of candidate samples composed of 1000 images. 1/3 from training, 1/3 from validation and 1/3 from test. For pairwise attacks, the comparison between synthetic and candidate is done in pixel space and embedding space. For the pixel space, similarity

is computed as the minimum Euclidean distance between one candidate and all the synthetic samples. The embedding distance is obtained by training a UMAP trained on 5000 images (3000 from the trainset, 1000 from the validation set, 1000 from the test set). The UMAP compresses the samples down to 64 features, the feature distance is obtained as the minimum Euclidean distance on features. For the distribution attacks, the threshold for 2 points to be considered as neighbours is that their distance is part of the 1st percentile.

7. Data and Code availability

The real datasets (F2305, A2209) used for training and testing are part of an ongoing clinical trial and not publicly shareable. Instead, a synthetic version of each datasets (with similar sample size and distribution) will be shared as a substitute. Paper code and synthetic datasets can be found at <https://github.com/tcoroller/pGAN>. Novartis is committed to sharing with qualified external researchers' access to patient-level data and supporting clinical documents from eligible studies. These requests are reviewed and approved based on scientific merit. All data provided are anonymised to respect the privacy of patients who have participated in the trial in line with applicable laws and regulations. The data may be requested from the corresponding author of the manuscript. The protocol would be made available on request by contacting the journal or the corresponding author.

8. Funding statement

The study was designed by the sponsor, Novartis, in collaboration with the authors. The institutional review board at each participating centre approved the protocol. Data were collected in accordance with Good Clinical Practice guidelines by the study investigators and were analysed by the sponsor. Agreements between the sponsor and the investigators included provisions relating to confidentiality of the trial data. All the authors vouch for the accuracy and completeness of the data and analyses, as well as for the fidelity of this study protocol, which are available from the funder.

9. Acknowledgements

The authors thank the patients who participated in this study and the study investigators for their contributions. The study was funded by Novartis Pharma AG, Basel, Switzerland, in accordance with Good Publication Practice (GPP3) guidelines (<http://www.ismpp.org/gpp3>).

References

- [1] J. De Fauw, J. R. Ledsam, B. Romera-Paredes, S. Nikolov, N. Tomasev, S. Blackwell, H. Askham, X. Glorot,

- B. O'Donoghue, D. Visentin, *et al.*, "Clinically applicable deep learning for diagnosis and referral in retinal disease," *Nature medicine*, vol. 24, no. 9, pp. 1342–1350, 2018. 1
- [2] B. Schmauch, A. Romagnoni, E. Pronier, C. Saillard, P. Maillé, J. Calderaro, A. Kamoun, M. Sefta, S. Toldo, M. Zaslavskiy, *et al.*, "A deep learning model to predict rna-seq expression of tumours from whole slide images," *Nature communications*, vol. 11, no. 1, pp. 1–15, 2020. 1
- [3] A. Hosny, C. Parmar, T. P. Coroller, P. Grossmann, R. Zeleznik, A. Kumar, J. Bussink, R. J. Gillies, R. H. Mak, and H. J. Aerts, "Deep learning for lung cancer prognostication: a retrospective multi-cohort radiomics study," *PLoS medicine*, vol. 15, no. 11, p. e1002711, 2018. 1
- [4] Y. Xu, A. Hosny, R. Zeleznik, C. Parmar, T. Coroller, I. Franco, R. H. Mak, and H. J. Aerts, "Deep learning predicts lung cancer treatment response from serial medical imaging," *Clinical Cancer Research*, vol. 25, no. 11, pp. 3266–3275, 2019. 1
- [5] "PubMed." <https://pubmed.ncbi.nlm.nih.gov>. 1
- [6] H. J. Smidt and O. Jokonya, "The challenge of privacy and security when using technology to track people in times of covid-19 pandemic," *Procedia Computer Science*, vol. 181, pp. 1018–1026, 2021. 1
- [7] J. M. Wing, "Ten research challenge areas in data science," *arXiv preprint arXiv:2002.05658*, 2020. 1
- [8] J. Cannataci, V. Falce, and O. Pollicino, *Legal Challenges of Big Data*. Edward Elgar Publishing, 2020. 1
- [9] J. L. Grama, *Legal and Privacy Issues in Information Security*. Jones & Bartlett Learning, 2020. 1
- [10] National Academies of Sciences, Engineering and Medicine and others, *Reproducibility and replicability in science*. National Academies Press, 2019. 1
- [11] F. Prior, K. Smith, A. Sharma, J. Kirby, L. Tarbox, K. Clark, W. Bennett, T. Nolan, and J. Freymann, "The public cancer radiology imaging collections of the cancer imaging archive," *Scientific data*, vol. 4, no. 1, pp. 1–7, 2017. 1
- [12] K. El Emam and L. Arbuttle, *Anonymizing health data: case studies and methods to get you started*. "O'Reilly Media, Inc.", 2013. 2
- [13] T. Ryffel, A. Trask, M. Dahl, B. Wagner, J. Mancuso, D. Rueckert, and J. Passerat-Palmbach, "A generic framework for privacy preserving deep learning," *arXiv preprint arXiv:1811.04017*, 2018. 2
- [14] I. J. Goodfellow, J. Pouget-Abadie, M. Mirza, B. Xu, D. Warde-Farley, S. Ozair, A. Courville, and Y. Bengio, "Generative adversarial networks," *arXiv preprint arXiv:1406.2661*, 2014. 2
- [15] T. Karras, S. Laine, and T. Aila, "A style-based generator architecture for generative adversarial networks," in *Proceedings of the IEEE/CVF Conference on Computer Vision and Pattern Recognition*, pp. 4401–4410, 2019. 2
- [16] L. McInnes, J. Healy, and J. Melville, "Umap: Uniform manifold approximation and projection for dimension reduction," *arXiv preprint arXiv:1802.03426*, 2018. 2
- [17] L. Van der Maaten and G. Hinton, "Visualizing data using t-sne," *Journal of machine learning research*, vol. 9, no. 11, 2008. 2
- [18] K. He, X. Zhang, S. Ren, and J. Sun, "Deep residual learning for image recognition," in *Proceedings of the IEEE conference on computer vision and pattern recognition*, pp. 770–778, 2016. 2
- [19] E. Tom, P. A. Keane, M. Blazes, L. R. Pasquale, M. F. Chiang, A. Y. Lee, and C. S. Lee, "Protecting data privacy in the age of ai-enabled ophthalmology," *Translational Vision Science & Technology*, vol. 9, no. 2, pp. 36–36, 2020. 6
- [20] S. Mukherjee, Y. Xu, A. Trivedi, and J. L. Ferres, "Protecting gans against privacy attacks by preventing overfitting," 2020. 6
- [21] C. Dwork, "Differential privacy: A survey of results," in *International conference on theory and applications of models of computation*, pp. 1–19, Springer, 2008. 6
- [22] J. Jordon, J. Yoon, and M. Van Der Schaar, "Pate-gan: Generating synthetic data with differential privacy guarantees," in *International Conference on Learning Representations*, 2018. 6
- [23] D. Chen, N. Yu, Y. Zhang, and M. Fritz, "Gan-leaks: A taxonomy of membership inference attacks against generative models," in *Proceedings of the 2020 ACM SIGSAC Conference on Computer and Communications Security*, pp. 343–362, 2020. 6
- [24] B. K. Beaulieu-Jones, Z. S. Wu, C. Williams, R. Lee, S. P. Bhavnani, J. B. Byrd, and C. S. Greene, "Privacy-preserving generative deep neural networks support clinical data sharing," *Circulation: Cardiovascular Quality and Outcomes*, vol. 12, no. 7, p. e005122, 2019. 6
- [25] S. Kazemina, C. Baur, A. Kuijper, B. van Ginneken, N. Navab, S. Albarqouni, and A. Mukhopadhyay, "Gans for medical image analysis," *Artificial Intelligence in Medicine*, p. 101938, 2020. 6
- [26] X. Yi, E. Walia, and P. Babyn, "Generative adversarial network in medical imaging: A review," *Medical image analysis*, vol. 58, p. 101552, 2019. 6
- [27] H.-C. Shin, N. A. Tenenholtz, J. K. Rogers, C. G. Schwarz, M. L. Senjem, J. L. Gunter, K. P. Andriole, and M. Michalski, "Medical image synthesis for data augmentation and anonymization using generative adversarial networks," in *International workshop on simulation and synthesis in medical imaging*, pp. 1–11, Springer, 2018. 6
- [28] C. Han, H. Hayashi, L. Rundo, R. Araki, W. Shimoda, S. Muramatsu, Y. Furukawa, G. Mauri, and H. Nakayama, "Gan-based synthetic brain mr image generation," in *2018 IEEE 15th International Symposium on Biomedical Imaging (ISBI 2018)*, pp. 734–738, IEEE, 2018. 6
- [29] S. Fossen-Romsaas and A. Storm-Johannessen, "Synthesizing skin lesion images using generative adversarial networks," Master's thesis, The University of Bergen, 2020. 6

- [30] M. Frid-Adar, I. Diamant, E. Klang, M. Amitai, J. Goldberger, and H. Greenspan, “Gan-based synthetic medical image augmentation for increased cnn performance in liver lesion classification,” *Neurocomputing*, vol. 321, pp. 321–331, 2018. 6
- [31] H. Zhang, Z. Huang, and Z. Lv, “Medical image synthetic data augmentation using gan,” in *Proceedings of the 4th International Conference on Computer Science and Application Engineering*, pp. 1–6, 2020. 6
- [32] Z. Wang, A. C. Bovik, H. R. Sheikh, and E. P. Simoncelli, “Image quality assessment: from error visibility to structural similarity,” *IEEE transactions on image processing*, vol. 13, no. 4, pp. 600–612, 2004. 8
- [33] D. Baeten, J. Sieper, J. Braun, X. Baraliakos, M. Dougados, P. Emery, A. Deodhar, B. Porter, R. Martin, M. Andersson, *et al.*, “Secukinumab, an interleukin-17a inhibitor, in ankylosing spondylitis,” *New England journal of medicine*, vol. 373, no. 26, pp. 2534–2548, 2015. 8
- [34] A. Jamaludin, T. Kadir, and A. Zisserman, “Spinenet: automated classification and evidence visualization in spinal mris,” *Medical image analysis*, vol. 41, pp. 63–73, 2017. 8
- [35] A. Odena, C. Olah, and J. Shlens, “Conditional image synthesis with auxiliary classifier gans,” in *International conference on machine learning*, pp. 2642–2651, PMLR, 2017. 8
- [36] D. P. Kingma and J. Ba, “Adam: A method for stochastic optimization,” *arXiv preprint arXiv:1412.6980*, 2014. 9
- [37] B. Efron, “Better bootstrap confidence intervals,” *Journal of the American statistical Association*, vol. 82, no. 397, pp. 171–185, 1987. 10

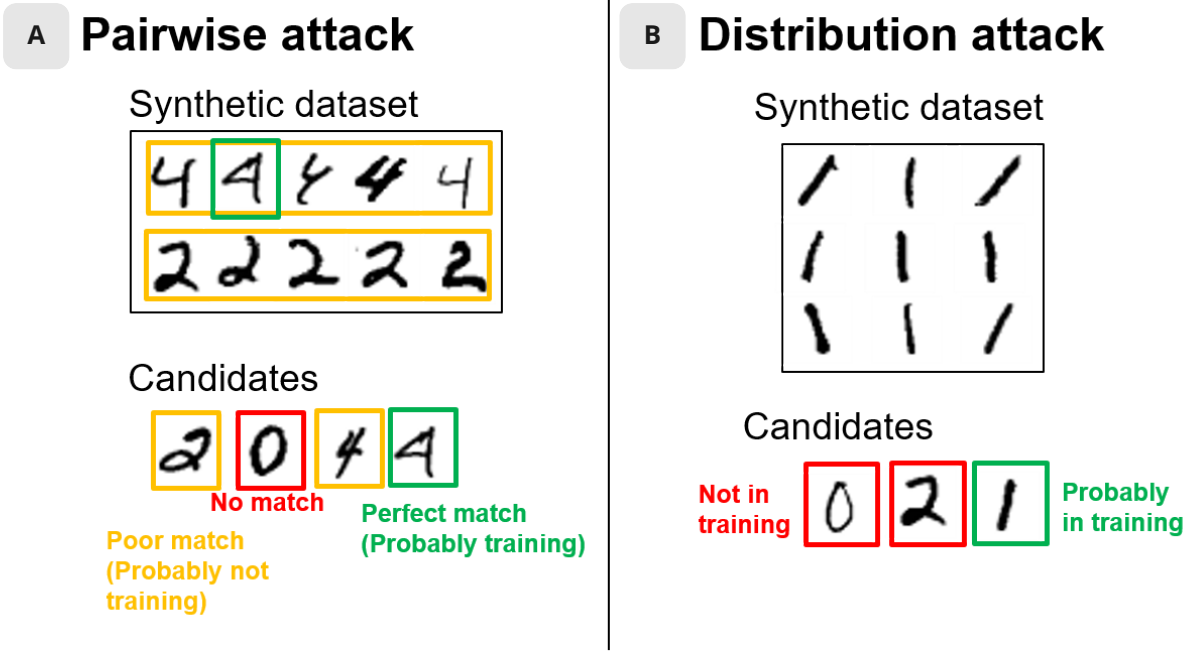


Figure S1: **Candidate pair definition.** Column A, example of a pairwise attack of a synthetic dataset. The green digit from candidates is closely matching the green digit from the synthetic dataset meaning this candidate is likely in the trainset and privacy is not preserved. Column B, example of a distribution attack on a synthetic dataset. While not being an exact match, the green digit is very similar to the digits from synthetic. This indicates that the green digit is likely present in the trainset.

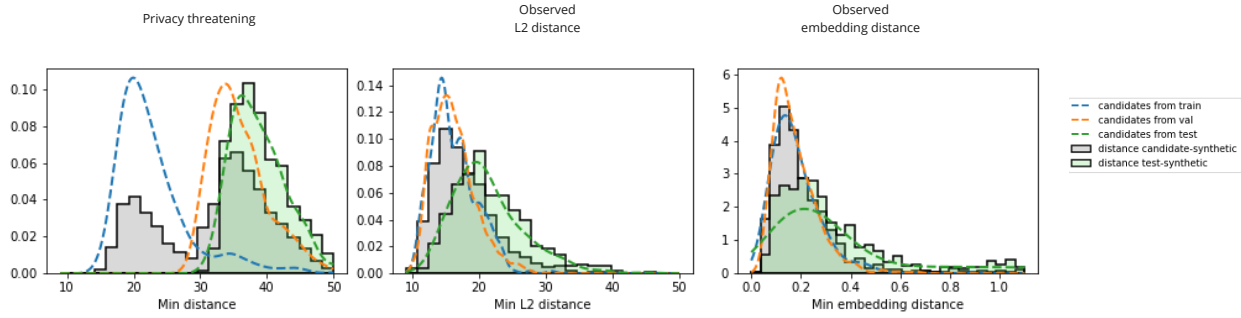


Figure S2: **Privacy attack scenarios.** In this experiment, the abnormally low distances between candidates and synthetic can be identified by anomaly detection. An abnormal sample is any sample that diverges largely from the distance test-synthetic (green distribution). For our synthetic dataset, validation samples are also classified as outliers, privacy is preserved.

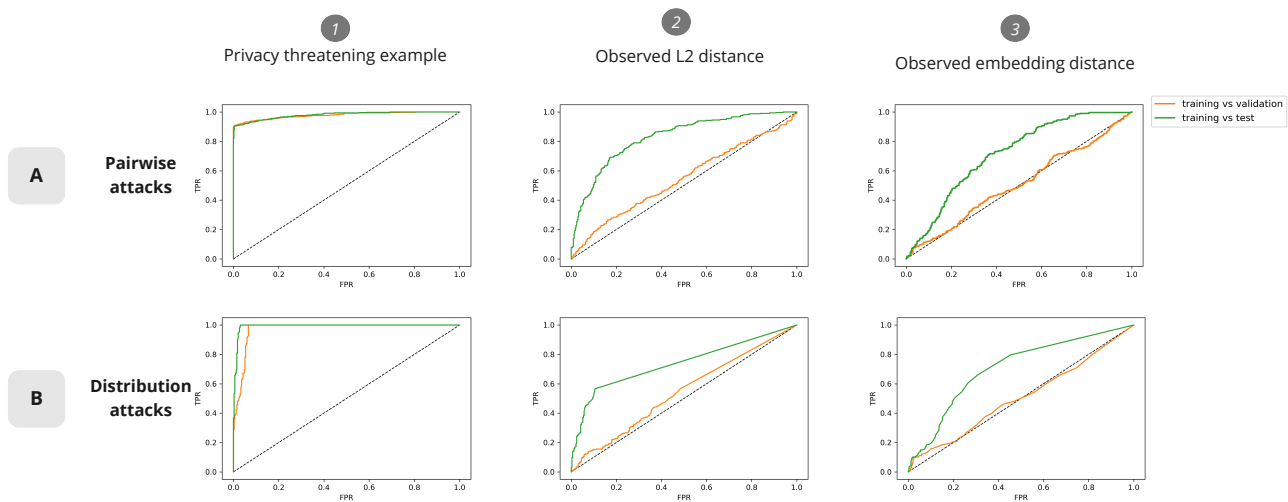


Figure S3: **ROC curves.** ROC for classification of candidate samples from train vs validation (orange) and train vs test (green). A) pairwise attacks. The classification is under the assumption candidates with the lowest distances are likely from training. B) Distribution attacks. The classification is done by associating large clusters to training samples. A high AUC means it is easy to classify training from other samples.

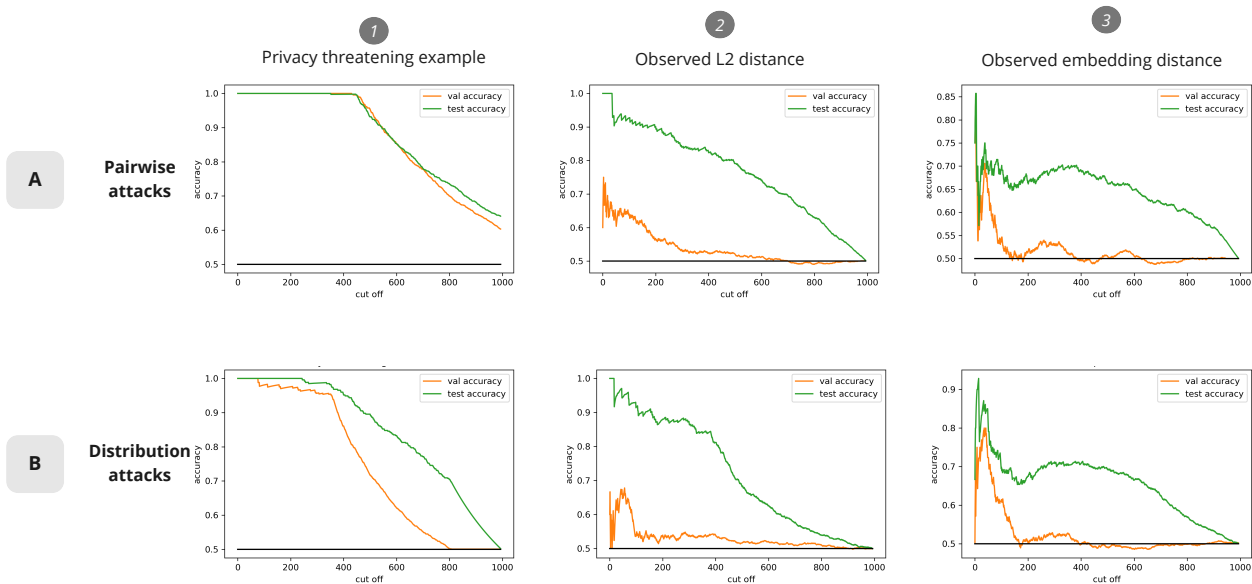


Figure S4: **Cut-off curves.** Cut off defines the threshold for a point to be considered an outlier. The curve orange shows the proportion of outliers from training vs outliers from validation. The green curve shows the proportion of outliers from training vs outliers from test. A privacy threatening case correspond to almost all of outliers coming from the training set.

	Pairwise attacks					
	Toy example		L2 distance		Embedding distance	
Cut off	50	333	50	333	50	333
Train proportion	1.00	0.89	0.58	0.48	0.51	0.43
Val proportion	0.00	0.04	0.36	0.43	0.27	0.38
Test proportion	0.00	0.07	0.05	0.09	0.22	0.19
	Distribution attacks					
	Toy example		L2 distance		Embedding distance	
Cut off	50	333	50	333	50	333
Train proportion	0.93	0.91	0.64	0.49	0.62	0.43
Val proportion	0.05	0.07	0.33	0.42	0.24	0.39
Test proportion	0.02	0.02	0.04	0.09	0.15	0.18

Table S1: **Classification of candidate origin.** Proportion of origin for different candidates at given cut-off. Cut off 50 means the top 50 largest clusters or smallest distances are considered outliers (50 is top 5% of the 1000 candidate images). In extreme privacy threatening scenarios, we expect that all training sample can be identified as outliers meaning they would represent 100% of the top 333 candidates.